MONTE CARLO MODELING OF THE YTTRIUM-90 NANOSPHERES APPLICATION IN THE LIVER RADIONUCLIDE THERAPY AND ORGANS DOSES CALCULATION

by

Seyed Mostafa GHAVAMI [1]***, Hosein GHIASI*** [1*]***, and Asghar MESBAHI*** [2]

[1] Department of Radiology, Paramedical School, Tabriz University of Medical Sciences, Tabriz, Iran
[2] Department of Medical Physics, Medical School, Tabriz University of Medical Sciences, Tabriz, Iran

Scientific paper
DOI: 10.2298/NTRP1601089G

Using the nano-scaled radionuclides in the radionuclide therapy significantly reduces the particles trapping in the organs vessels and avoids thrombosis formations. Additionally, uniform distribution in the target organ may be another benefit of the nanoradionuclides in the radionuclide therapy. Monte Carlo simulation was conducted to model a mathematical humanoid phantom and the liver cells of the simulated phantom were filled with the ^{90}Y nanospheres. Healthy organs doses, fatal and nonfatal risks of the surrounding organs were estimated. The estimations and calculations were made in four different distribution patterns of the radionuclide seeds. Maximum doses and risks estimated for the surrounding organs were obtained in the high edge concentrated distribution model of the liver including the nanoradionuclides. For the dose equivalent, effective dose, fatal and non-fatal risks, the values obtained as 7.51E-03 Sv/Bq, 3.01E-01 Sv/Bq, and 9.16E-01 cases/10^4 persons for the bladder, colon, and kidney of the modeled phantom, respectively. The mentioned values were the maximum values among the studied modeled distributions. Maximum values of Normal Tissue Complication Probability for the healthy organs calculated as 5.9-8.9 %. Result of using nanoparticles of the ^{90}Y provides promising dosimetric properties in MC simulation results considering non-toxicity reports for the radionuclide.

Key words: nanoscaled ^{90}Y, internal dosimetry, organs absorbed dose, risk estimation, radionuclide therapy

INTRODUCTION

Nowadays, radiation therapy has been established as a choice of the cancer treatment or palliation beside the chemotherapy and surgery. To deliver the prescribed radiation dose to the target site with a nearby source, the high dose rate and rapid dose drop off after cancerous region has been great advantages for radionuclide therapy sources. In some cases, like liver metastasis, internal radionuclide therapy is the best choice for the cancer treatment and management. In the radionuclide therapy technique, optimization of the methods and sources requires detailed study of the sources dosimetric characteristics and methods advantages and pitfalls before clinical implementation. Some researchers have conducted studies on the sources energy, sources size effects on the treatment quality as well as the configuration of the sources implantation [1-6]. Otherwise, there are many ongoing researches on the application of the radionuclides in the cancer treatment and palliation. Some of the radionuclides have been verified and validated as good radiation therapy outcome. In case of the yttrium-90 (^{90}Y) radionuclide, high linear energy transfer (LET) factor of the β^- particles emitted from the radionuclide rather than photons and distribution of the nanoscaled particles may be effective in the metastases removing. The liver is unique in having two blood supplies – an artery (the hepatic artery) and a large vein (the portal vein). The normal liver gets about 75 % of its blood from the portal vein and only 25 % of its blood comes from the hepatic artery. When a tumor grows in the liver, it may receive almost all of its blood supply from the hepatic artery. ^{90}Y microspheres are injected as beads with the radioactive material directly into the arteries supplying the blood to the liver tumor site. Since the beads are placed directly into the tumor vessels, it does not have the profound impact on the body when compared to other therapies such as systemic chemotherapy. Using the nano-scaled radionuclides might have potential advantages in this regard. Using radionuclide therapy for the liver tumors killing may offer promising results in the treatment quality and outcome because the external whole liver radiotherapy might impose a dose to the liver's normal parenchyma.

* Corresponding author; e-mail: hoseinghiasi62@gmail.com

Toxicity of ^{90}Y-microspher radionuclide therapy after the intra-arterial radionuclide therapy has been studied and reported its toxicity in grade 3-4 tumors treatment lower for clinical study than laboratory findings [7-14]. We conducted the current study to finding out if using ^{90}Y nanospheres instead of its microspheres offers the patient undergoing liver radionuclide therapy any advantage? Although it is obvious that the probability of the radionuclide particles trapping in the liver vessels reduces significantly according to the particles size reduction. Additionally, distribution of the nanoparticles will be relatively uniform rather than microspheres. But, it is important to find out dosimetric advantages of the nano-scaled radionuclide. On the other hand, in addition to the uniform distribution and low probability of the particles trapping, the dose distribution around the radioactive particles filled liver was important in this study. For this reason, in addition to the liver absorbed dose characterization, a dose to the surrounding organs was calculated and normal tissue complication probability (NTCP) was found for the organs. Finally, advantages and disadvantages of using the nanospheres were discussed.n this study, the patient organs doses from the ^{90}Y nanoradionuclide injected to the liver for the metastases treatment werestudied and estimated. Fatality and non-fatal risks associated with the nanoparticle for the surrounding organs were also studied in the current study.

MATERIALS AND METHODS

MCNPX (2.6.0) code of Monte Carlo (MC) released by the Los Alamos national laboratory (LANL) was used in all simulations and calculations carried out for this study. For the patient organs simulation, a mathematical-based adult phantom was manipulated so that the ^{90}Y nanoparticles modeled as a filled lattice resembling the radionuclide therapy radiation sources in the phantom's simulated liver. Size of the modeled radionuclide nanospheres considered to be 4 nanometers (4 10^{-9} m) and each side of the voxels in the liver modeled as 1 micrometer (1 10^{-6} m). For making our estimations closer to the realistic situation, four different patterns of the radionuclide distribution in the liver were considered in the simulations. Distribution of the ^{90}Y radionuclides in the liver was considered as uniform, highly concentrated in the center, increasing the concentration from the center toward the edges and with irregular distribution. The modeled ^{90}Y radionuclide was β^- emitter with the E_{Max} of 2.28 MeV and its half-life was considered 64 hours in the calculations. Additionally, energy spectrum of the nanoradionuclides was modeled so they were emitted β^- particles with E_{mean} equal to 0.651 MeV in the isotropic radiation emission pattern. As we know the ^{90}Y is produced by the neutron activation according to the ^{89}Y$(n, \gamma)^{90}$Y nuclear reaction. The activated radionuclide is associated with the specific activity of 400 MBq/mg. It decays through pure β^- emission to the stable state of ^{90}Zr. For our model benchmarking and validation, normalized specific absorption fraction (SAF) for an initial particle of the emitted β^- nanoradionuclides was calculated and compared with the published data. Modeling the liver as the source of β^-, the particles and produced photons from β^- interactions with surrounding material were simulated and absorption fraction in the liver and kidney (for β^-) and lung for the photons were calculated and plotted – figs.1 and 2 show the results. It was seen as a good agreement between our derived data and published data. Thus, comparison of the results with the published data benchmarked our mode for using for the calculations [15-20].

Using the simulation results, absorbed dose equivalent, effective dose, fatal and non-fatal risks due to the radiation, the doses were estimated for the patient organs as the guidelines and tabulated in tab. 1.

$$D \quad \frac{\mathrm{d}\bar{\varepsilon}}{\mathrm{d}m} \tag{1}$$

where, the mean value of dε (in J) is the mean energy imparted to matter of mass dm (in kg) by ionizing radiation and a special name given to D is (Gy). In the microdosimetry where dm is very small, imparted en-

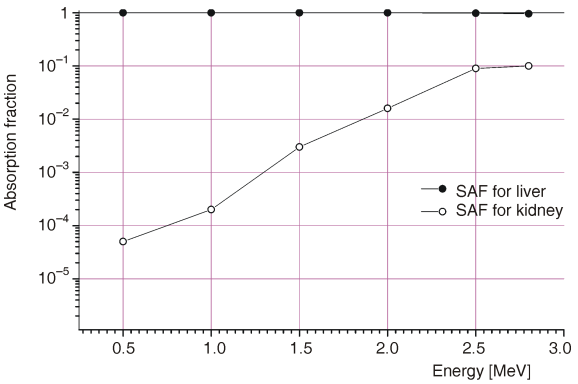

Figure 1. Calculated SAF for liver and kidney in our modeling. The values were derived in the uniform distribution of nanoradionuclide in the liver

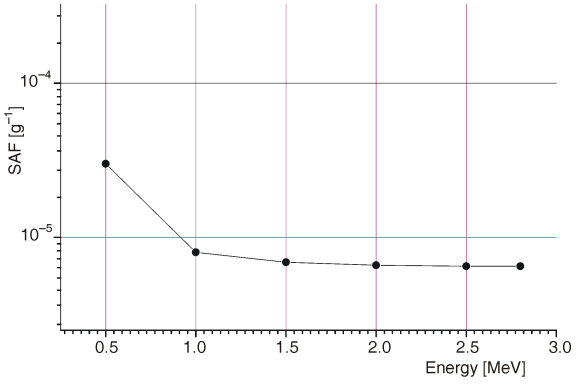

Figure 2. Calculated SAF for the lung of used phantom

Table 1. Organ doses and risk estimation in the liver ^{90}Y radionuclide therapy

Organ	Dose equivalent [SvBq^{-1}]	Non-fatal risk (cases per 10,000 persons per Sv)	Fatal risk (cases per 10,000 persons per Sv)	Nominal risk adjusted for lethality and quality of life
1. Ovaries	7.34E-01	1.69E-02	1.210E-02	6.46E-02
2. Leg bones	1.63E-03	6.36E-03	5.22E-03	8.31E-03
3. Arm bones	4.78E-03	1.86E-03	1.53E-03	2.44E-03
4. Pelvis bones	7.54E-03	2.94E-03	2.41E-03	3.85E-03
5. Spine bones	4.65E-03	1.81E-03	1.49E-03	2.37E-03
6. Skull bone	4.95E-03	1.93E-03	1.58E-03	2.52E-03
7. Spine bone	4.65E-05	1.81E-03	1.49E-03	2.37E-03
8. Skull bone	4.95E-03	1.93E-03	1.58E-03	2.52E-03
9. Rib cage bone	6.59E-03	2.57E-03	2.11E-03	3.36E-06
10. Clavicles bone	8.36E-03	3.26E-03	2.68E-02	4.26E-02
11. Scapulae	2.26E-03	8.81E-03	7.23E-03	1.15E-02
12. Colon	1.12E-03	3.83E-03	3.51E-03	5.53E-03
13. Lungs	6.42E-03	8.09E-03	6.52E-03	7.25E-03
14. Stomach	4.05E-01	5.47E-02	2.65E-02	3.12E-02
15. Bladder	1.35E-01	4.19E-02	1.62E-02	3.17E-02
16. Breasts	1.83E-02	1.45E-02	6.04E-03	1.13E-02
17. Liver	8.36E-01	4.70E-01	9.71E-01	1.01E+00
18. Esophagus	1.38E-01	2.49E-01	3.19E-02	3.41E-02
19. Thyroid	3.09E-03	9.36E-02	6.80E-03	3.03E-02
20. Skin	2.07E-05	2.07E-02	4.14E-05	8.28E-05
21. Adrenals	3.92E-03	1.44E-02	1.38E-02	4.32E-01
22. Brain	4.49E-05	1.65E-04	1.58E-04	4.95E-03
23. Kidney	4.49E-05	1.65E-04	1.58E-04	4.95E-03
24. Pancreas	6.78E-04	2.48E-03	2.39E-03	7.47E-02
25. Spleen	3.50E-04	1.28E-03	1.23E-03	3.86E-02
26. Thymus	3.06E-03	1.12E-02	1.08E-02	3.37E-01
27. Uterus	8.10E-04	2.97E-03	2.86E-03	8.93E-02

ergy is taken to account instead of its mean value. Then, D has fluctuations in small masses and the fluctuations increase with the absorber mass decreasing. But, in our applied scale, the mean value of the imparted energy is inserted in the equation.

Equivalent dose (H) in Sv is calculated by the production of D and radiation weighting factor w_R as

$$H_T \quad \underset{R}{} w_R D_{T,R} \tag{2}$$

where w_R is different for different type and energy of radiation. Its value recommended for the photon and electron in all of energies as 1. $D_{T,R}$ is the dose in a point due to the radiation R in an organ or tissue T. Effective dose formulation has been recommended as

$$E \quad \underset{T}{} w_T \underset{R}{} w_R D_{T,R} \tag{3}$$

where w_T and w_R are tissue weighting factor and radiation weighting factor, respectively. $D_{T,R}$, is the point dose due to the radiation field R in a tissue T. The unit of E is same as H and is Sv.

Fatal and non-fatal risks were calculated using the obtained effective dose and ICRP [21] tabulated nominal risk per Sv in 10^4 persons. The studied organs included testes ovaries, pancreas, genitalia, leg bones, arm bones, pelvis bone, spine bone, skull bone, rib cage bone, clavicles bone, scapulae, colon (large intestine), lungs, stomach wall, bladder, breasts, liver, esophagus, thyroid, skin, adrenals, brain, kidney, muscle, spleen, thymus, and uterus. Using our MC model the absorbed dose was calculated for the different organs. Energy deposition in the organs was obtained in terms of MeV and converted to the J/kg unit which is equal to the unit of absorbed dose (Gy). The absorbed dose obtained per particle emission (Gy/Bq) and considering the total β^- emission from the nanosources, absorbed dose for each of the organs was tallied. Additionally, maximum range of the emitted β^- particles in the liver tissue was calculated by the MC simulation. Because we assumed that for the radioactive ^{90}Y filled liver, the interaction of the emitted particles with the atoms in the liver cells and surrounding tissues may produce Bremsstrahlung-ray, then, the photon spectra were also tallied at the modeled liver cell in the low energies and narrow energy bins. The spectrum was derived by the F4 tally and determining the energy bins in which the photon numbers would be tallied in data card of the written input file. Derived produced X-ray spectrum in the liver tissue was shown in fig. 3. The results tabulated in tab. 1 obtained for the nanoparticles uniform distributed condition. The same values were calculated for the other patterns of distribution and the results were compared. Because of the fact that the sur-

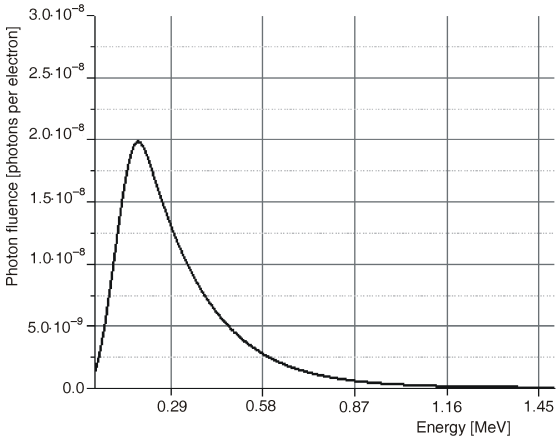

Figure 3. MC derived the β^- particle produced bremsstrahlung X-ray photons spectra at the modeled liver

rounding organs may be exposed more than those that are far from the liver, normal tissue complication probability (NTCP) for the organs near the sources were calculated according to the obtained data and recommended method as presented by the following formulation of the relative seriality model. Below equations were used for the organs NTCP calculation. The probability for controlling a tumor or tumor control probability (TCP) can be calculated using the following equation [16]

$$P(D) \quad e^{e^{\gamma \quad (nd/D_{50})(e\gamma \quad \ln \ln 2)}} \tag{4}$$

$P(D)$ is the probability of tumor in an organ. D_{50} is the dose for which the response is 50 % and γ is the maximum normalized value of the dose response gradient. The parameter n is the number of fractions. Tumor control probability (TCP) for a heterogeneous tumor in an organ is defined in eq. (5).

$$TCP \quad \prod_{i}^{N} P_i(D)^{\Delta v_i} \tag{5}$$

Normal tissue complication probability for both serial and parallel tissues can be calculated from

$$NTCP \quad 1 \quad \prod_{i}^{N} [1 \quad P_i(D)^s]^{\Delta v} \quad ^{1/s} \tag{6}$$

In eq. (6) for NTCP calculation, s is the parameter describing the tissue structure (serial or parallel). NTCP for the liver and surrounding organs were calculated using the described formulations [16]. The spectra were derived for each of the studied radionuclide distribution separately and compared. Dose absorption in the energy bins was tallied for both of the irradiations.

RESULTS

Our MC code calculation results estimated the patient's organs doses, effective doses, fatal and non-fatal risks estimations, in the liver ^{90}Y nanoradionuclide therapy.Interactions between the ^{90}Y radionuclides and tissue produced low energy Bremsstrahlung X-ray. From the fig. 1, peak of the produced Bremsstrahlung X-ray photons lies around 240 keV. Additionally, both X-ray photons and nanoradionuclides emitted β^- particles spectra at the spine bone surface were derived by the MC simulation and were shown in fig. 2. Then, the liver filled by the ^{90}Y nanoradionuclides can be considered as β^- and X-ray source and photons spectra were shown in fig. 3. Some of the Bremsstrahlung photons deposit their energy far from the production origin. Then, a dose of some organs that are far from the liver was also calculated. Radiation spectra at the spine bone surface were derived for β^- and X-ray photons and were shown in fig. 4. After the tissue included the radiation sources, ovaries absorbed maximum dose in uniform distribution model of the sources in the liver. Our code calculation results showed dose absorption and the estimated risks higher for the distribution in which the radionuclide concentration is high in the liver edges. Absorbed dose equivalent, fatal and non-fatal estimated risks values were obtained in the uniform distribution as $7.34 \cdot 10^{-3}$ Sv/Bq, $9.71 \cdot 10^{-2}$ Sv/Bq, and $4.71 \cdot 10^{-1}$ cases per 10^4 persons for the ovaries, liver and liver, respectively. The values were obtained for the high edge-concentrated model as $7.51 \cdot 10^{-3}$ Sv/Bq, $3.01 \cdot 10^{-1}$ Sv/Bq, and $9.16 \cdot 10^{-1}$ cases per 10^4 persons

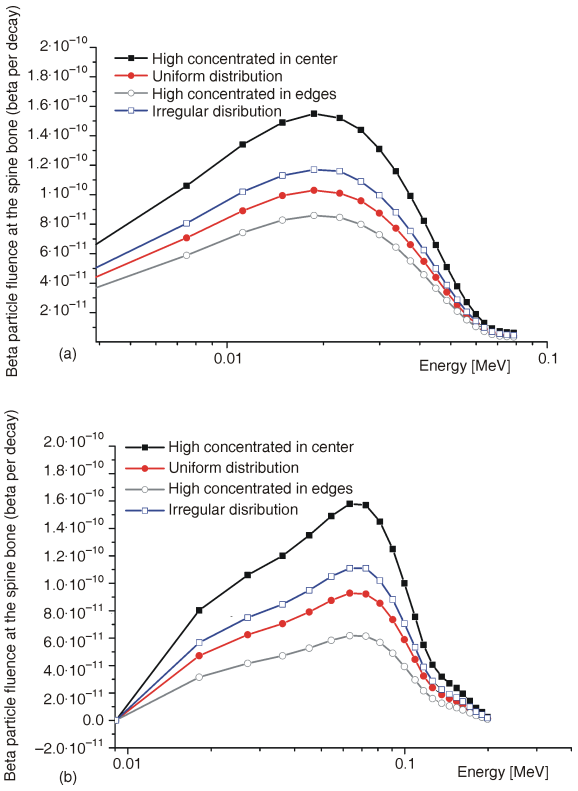

Figure 4. β^- particles spectra at the spine bone (a), and β^- particles produced Bremsstrahlung X-ray photons spectra at the spine bone (b)

Table 2. Comparison of doses and the estimated risk between the studied modeled distributions of the radionuclide particles in liver

Distribution model	Distribution (1) (uniform concentration)	Distribution (2) (concentration in liver's edges)	Distribution (3) (concentration in liver's center)	Distribution (4) (irregular concentration)
Maximum dose equivalent (Sv)	7.34E-03 (ovaries)	7.51E-03 (bladder)	7.09E-03 (spine bone)	7.29E-03 (ovaries)
Maximum effective dose (Sv)	3.67E-04 (ovaries)	3.75E-04 (bladder)	7.09E-05 (spine bone)	3.64E-04 (ovaries)
Maximum estimated fatal risk (cases/10^4persons/Sv)	2.65E-02 (stomach)	3.01E-02 (colon)	2.28E-02 (adrenals)	2.69E-02 (stomach)
Maximum estimated non-fatal risk (Cases/10^4persons/Sv)	9.36E-02 (thyroid)	1.16 E-01(kidney)	8.93E-02 (colon)	9.31E-02 (thyroid)

for the bladder, colon and kidney of the modeled phantom respectively. Table 2, shows the maximum values obtained in the high concentration in the edges of the liver condition. In contrast, lower values were obtained for dose and risk estimation calculated in central concentrated modeled liver among the studied models of distribution. Among the modeled distributions, irregular and uniform filled liver showed good agreement in the result of dose and risk calculations rather than the others. Table 2 shows that only slight difference is between the two irregular and uniform radionuclide distributions models results. As the modeling of the distribution pattern in the real case is nearly impossible because of person to person variations in distribution, considering uniform filled liver with the nano ^{90}Y sources may be good estimator model for the surrounding organs doses calculation.As it can be seen in fig. 5, photons have energy less than 100 keV and photoelectric phenomenon has high cross-section in this energy range with bone. Additionally, when the radionuclide particles were concentrated at the center of liver, more beta particles interacted with tissue and more photons produced in the liver. Then, the liver as a virtual photon point like source emits more photons. In contrast, both of the radiation fluence had minimum value when the nanoparticles are concentrated in the edges of liver. In addition, a slight shift can be seen in the peak of energy of both photon and beta spectra. Dose distribution in the narrow energy bins was derived for the spine bone in both photon and beta irradiation originating from the liver. Figure 5 shows the absorbed dose distribution in the energy bins.

Our study considered the received dose in two parts; dose from the β^- particles emitted from the nanoparticles and X-ray produced in the emitted particles and tissue interactions. The results showed that around 34 % of the bone absorbed dose was due to the beta particles and 66 % originated from the X-ray photons. Because spine bone is closer to the liver than the other studied organs and beta particles expect to have higher portion in the irradiation field rather than those at greater distances from the liver, it may be deduced that X-ray has the main role in distant organs irradiation

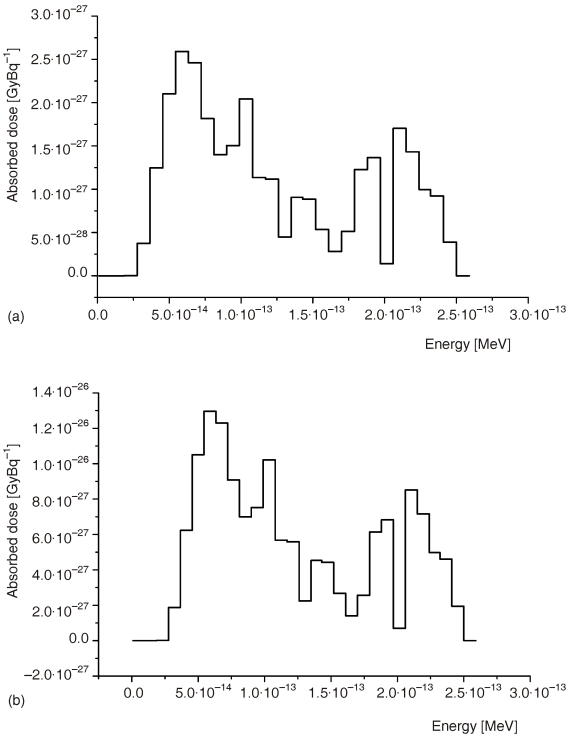

Figure 5. Absorbed dose spectra at the spine bone from the emitted β^- particles (a) and absorbed dose spectra at the spine bone from the emitted β^- particles produced bremsstrahlung X-ray photons (b)

such as brain. 8.9 %, 5.9 %, and 8.7 % of NTCP were obtained for ovaries, bladder and spine bone,respectively. For the target organ, liver, it obtained as 31 %. Figure 1 shows that almost all of the nanoradionuclides emitted energy was absorbed in the target organ (liver). Figure 5 shows the value of dose absorption in narrow energy bins. Total doses for the studied organs are also tabulated in the results section.

DISCUSSION

This means that other organs, those located at distances greaterthan 11.98 mm from the liver were exposed by the photons produced at the β^- interactions with the body atoms.Owing to a distance from the liver edge and

according to the emitted particles maximum range, ovaries are not exposed to β^- particles and the produced photons can reach to ovaries, while for the center filled liver model of ^{90}Y distribution bone surface showed absorbed maximum dose equivalent. It may be attributed to the fact that the bones are nearby and on the other hand, low energy of the photons and high atomic number of the tissue has led to photo-electric effect with high cross-section. Auger electrons and characteristic X-ray production also participate in the bone dose. High atomic number of bone and low energy of the photons provided a condition in which the photo-electric predominantly occurred and the ejected photoelectrons could be highly absorbed in the bone tissue. According to the results, it can be seen that the non-fatal risks is higher than fatal risks. It may be because of the fact that non-fatal risks include all of the stochastic effects such as heredity effects. In the low doses, deterministic effects which lead to death do not occur, but the secondary induced non-fatal malignancies and heredity risk induction is dominant. Mass and consequently concentration of the required radionuclide for delivering 30 Gy dose to the liver can be obtained from its specific activity. It can be deduced from the results that modeling the uniform distribution may give good results that are relatively close to real estimation of the organs doses and the associated risks. The agreement may be due to the fact that the resultant of the irregular diffusion of the nanoparticles in the liver tissue is close to a uniform one in case of the surrounding organs irradiation. For β^- and photon irradiation of the other organs, the liver may be considered as a virtual point like isotropic source. This hypothesis may be an explanation to why the results were close in the two distribution models. This agreement can also be seen in the radiation fluence at the spine bone surface in the four distributions study. In some cases, there are differences in the organs with maximum dose values. The difference can be attributed to the fact that displacement of the radionuclides concentration from the center to edges of the liver can lead to difference in the virtual source characteristics as mentioned above. Considering the β particles maximum range of 12 cm in the soft tissue and produced X-ray photons displacement of the beta particles and photons origin may alter the other organs received dose. The shift may be attributed to the radiation sources origin shift from the center toward the edge and *vice versa*. The fluence in case of both photon and beta radiations is in good agreement for the uniform and irregular distribution models rather than the others. This result shows that the resultant of the irregular pattern of the radionuclide distribution is close to the uniform one. Then, even if the sources distribute irregularly, a uniform modeling can estimate the result relatively precisely rather than the other patterns. Of the patient organs, spine bone received the maximum dose equivalent in one of the studied models. Then, it may be true to say that the distant organs received dose completely from the X-ray photons. According to the radiation dose tolerance of the studied organs and obtained doses, if we consider 30 Gy dose to be delivered to the liver for avoiding the induced-diseases, none of the organs receive a dose more than its tolerance. But, secondary induced malignancies may be observed in the follow -up program. Highest fatal and non-fatal risk was seen for the colon and stomach, respectively, and minimum fatal and non-fatal risk was calculated for the leg bones of the patient. Then, radiation induced hereditary complications and secondary cancers may be observed in the long run after treatment. Analytical NTCP calculation conducted for the organs received highest dose. According to the calculations, NTCP obtained for ovaries, bladder, and spine bone were 8.9 %, 5.9 %, and 8.7 %, respectively. Those results showed that the maximum NTCP using the ^{90}Y nanoradionuclides injected to the liver is 5.9-8.9 %. Those values for the NTCP while the liver metastases are treated is low. For the liver as the organ involved with the cancer and to be treated, NTCP found was 31 %. Considering the deleterious effect of the radionuclide on the cancer cells and the induced complications in the liver tissue, the nanoradionuclide seems to be an effective treatment method for the liver cancer treatment or palliation. Almost all of the radionuclides emitted energy was absorbed in the target organ. Calculated NTCP for the organ filled by the radionuclide (target organ) is low and comparing the benefits and complication probability of liver shows that the nanoradionuclides toxicity is acceptable and low. In the current work, we studied and evaluated physically in details the nanoradionuclide injection into the cancerous liver by the MC simulation. Obtained data can be used injustifying that the method's benefits outweighits hazards to the patient healthy organs. In the current study, size of the radionuclides in nanoscale was 4 nm, which offered advantages such as nearly uniform distribution and significant reduction in the probability of the thrombosis occurrence and entrapment of the particles at the vessels. Our study has major differences from the other similar studies in this regard. Two radiation sources of beta particles and produced X-ray photons were considered in peripheral organs dose calculations. Also the current study dealt with different distributions of the sources in the tissue and each of the conditions led to different results. Additionally, our calculations were not only about the organs doses, but also the risks associated with the organs due to the absorbed dose were studied. And, it should be mentioned here that the radionuclides were studied in nanoscale rather than micro-scale. This comparison between the studies reveals the effect of the sources size on the dose distribution. Besides, in our point of view the nanoscale size of the radionuclide offers an important advantage for this type of treatment; as the larger particles may cause obstructions and blocking the vital vessels. On the other hand, precise data scoring around the radionuclide therapy sources and the radiation toxicity is important in terms of treatment outcome and providing more reliable criteria for treatment selection [7, 16, 22-32].

CONCLUSIONS

This study presents the results of the healthy organs doses and secondary radiation induced fatal and non-fatal risks estimation in the liver radionuclide therapy with ^{90}Y nanoparticle. The nanosources four different distributions studied and the results compared led us to a conclusion

that the irregular and uniform distribution results are close in the organs doses and risk estimation. Based on those results, we propose that modeling the uniform filled organ in the radionuclide therapy can be good agreement with the real case data. Additionally, according to the data obtained, NTCP of the studied radionuclide is low both for the healthy organs and the cancerous liver. On the other hand, we concluded from the results that the healthy organs doses were similar due to the Bremsstrahlung X-ray produced in the beta particles and tissues. We found that in the liver filled with the nanoradionuclides, surrounding organs were irradiated by two radiation sources; β^- and photons. In addition, it can be deduced that the main radiation field imposed excess dose to the distant organs was the photon radiation. Overall, we concluded that the nanoscaled studied radionuclide is a good choice for liver metastases and other organs NTCP was low. Then, we propose ^{90}Y nanoradionuclide as a good radiation source for the removing of liver metastases. Future studies and clinical trials are proposed to finding out more detailed and precise data in the studied nanoradionuclides use. In addition, dose distribution and side effects were satisfactory.

ACKNOWLEDGEMENTS

The authors would like to thank Tabriz University of Medical Sciences research affairs.

AUTHORS' CONTRIBUTIONS

Main idea of this work was developed by H. Ghiasi. The paper text was written by A. Mesbahi and S. M. Ghavami.

REFERENCES

[1] Moore, S., Park, M. A., Mueller,S., Activity Estimation Performance in Y-90 Microsphere Bremsstrahlung SPECT, *Journal of Nuclear Medicine, 50* (2009), 2, pp. 1433-1437
[2] Zhou, J., *et al*., Dosimetry of Y-90 Liquid Brachytherapy in Dogs with Osteosarcoma Using PET-CT, *Journal of Nuclear Medicine, 52* (2011), 1, pp. 1-129
[3] Yankevich, U., *et al*., Y-90 Microspheres Treatment Response Monitoring: PET/CT or Diagnostic MR?, *Journal of Nuclear Medicine, 56* (2015), 3, pp. 1335-1339
[4] Moore, S., *et al*., Measurement of Y-90 Resin Microsphere Activity Using Dose Calibrators, *Journal of Nuclear Medicine, 48* (2007), 2, pp. 70-74
[5] Wahidi, J., *et al*., Y-90 Sir-Sphere Treatment of Liver Cancer and Alternative Imaging Methods, *Journal of Nuclear Medicine, 55* (2014), 1, pp. 2706-2710
[6] Rhymer, S., Parker, J. A., Palmer, M., Detection of Y-90 Extravasation by Bremsstrahlung Imaging for Patients Undergoing Yttrium-90-ibritumomab Tiuxetan (Zevalin) Therapy, *Journal of Nuclear Medicine, 49* (2008), 1,pp. 417-424
[7] Bozkurt, M., *et al*., Value of FDG-PET at 4 Weeks After Y-90 Resin Microsphere Therapy for Early Response Evaluation, *Journal of Nuclear Medicine, 50* (2009), 2, pp. 1618-1624
[8] Civelek, A., SIRS-Spheres (Y-90 Microspheres) Therapy for Unrespectable Metastatic Liver Disease: Pitfalls from Tracer Preparation for Injection to Image Interpretation, *Journal of Nuclear Medicine, 52* (2011), 1, pp. 1082-1086
[9] Frey, E., *et al*., Estimation of Post-Therapy Marrow Dose Rate in Myeloablative Y-90 Ibritumomab Tiuxetan Therapy, *Journal of Nuclear Medicine, 47* (2006), 1, pp. 156-161
[10] Grana, C., *et al*., High Dose Y-90-Ibritumomab-Tiuxetan with Autologous Stem Cell Transplantation in Refractory-Resistant NHL Patients, *Journal of Nuclear Medicine, 51* (2010), 2, pp. 172-175
[11] Kucuk, O., *et al*., Y-90 Microsphere Therapy in Patients with Hemangioendothelioma, *Journal of Nuclear Medicine, 50* (2009), 2, pp. 1106-1112
[12] Maza, S., *et al*., Y-90 Ibritumomab Tiuxetan Treatment in Primary Cutaneous B-Cell Lymphomas: Initial Results of a Prospective Study, *Journal of Nuclear Medicine, 47* (2006), 1, pp. 99-106
[13] Mueller, S., *et al*., Dosimetric Considerations for the Radioembolisaton of Hyperperfused Liver Tumors with Y-90 Microspheres, *Journal of Nuclear Medicine, 49* (2008), 1, pp. 386-391
[14] Mueller, S., *et al*., Y-90 Microsphere Dosimetry in Hepatic Malignancies, *Journal of Nuclear Medicine, 50* (2009), 2, pp. 210-217
[15] Kratochwil, C., *et al*., Selective Arterial Administration of Y-90 and Lu-177 Labeled DOTATOC in the Treatment of Patients with a Gastroenteropancreatic Neuroendocrine Tumor, *Journal of Nuclear Medicine, 51* (2010), 2, pp. 334-340
[16] Mueller, S., *et al.*, Comparison of Y-90 SIRT Dosimetry Strategies Based on Modeling Normal Tissue Complication Probability (NTCP), *Journal of Nuclear Medicine, 51* (2010), 2, pp. 13-19
[17] Zhang, Z., *et al.*, Results of Y-90 SIR-Spheres Treatment of Unrespectable Hepatic Metastatic Carcinoid and Neuroendocrine Tumors, *Journal of Nuclear Medicine, 48* (2007), 1, pp. 37-43
[18] Zhang, Z., *et al*., Y-90 SIR-Spheres Treatment of Unrespectable Hepatic Metastatic Carcinoid and Neuroendocrine Tumors (NET), *Journal of Nuclear Medicine, 49* (2008), 1, pp. 116-121
[19] Zhang, Z., *et al*., Y-90 SIR-Sphere Treatment of Unrespectable Liver Cancers, *Journal of Nuclear Medicine, 51* (2010), 2, pp. 161-168
[20] Zhang, Z., *et al*., Comparison of Therapeutic Response Using RECIST Criteria: Y-90 SIR-Spheres and TheraSphere Treatment of Unrespectable Hepatocellular Carcinoma, *Journal of Nuclear Medicine, 54* (2013), 2, pp. 224-230
[21] ***, International Comission on Radiological Protection. ICRP ann (2007), ICRP 103, pp. 1-34
[22] Anand, A., *et al*., Y-90 PET and Bremsstrahlung: Parameters for Optimal Imaging Post-Radioembolic Therapy, *Journal of Nuclear Medicine, 52* (2011), 2, pp. 1079-1085
[23] Barber, T., *et al*., The Feasibility of PET/CT Imaging in Y-90 Radiation Synovectomy: Initial Experience, *Journal of Nuclear Medicine, 53* (2012), 1, pp. 2174-2181
[24] Baur, B., *et al*., Zr-89-, Y-90- and Lu-177-Labeling and Biological Testing of Mesoporous Silica Based Nanoparticles, *Journal of Nuclear Medicine, 56* (2015), 3, pp. 1064-1071
[25] Frey, E., *et al*., Estimation of Post-Therapy Marrow Dose Rate in Myeloablative Y-90 Ibritumomab

Tiuxetan Therapy, *Journal of Nuclear Medicine, 47* (2006), 1, pp. 156-161
[26] Jiang, M., *et al*., Characterization of Extrahepatic Distribution of Tc-99m Macroaggregated Albumin (MAA) on Hepatic Perfusion Imaging Studies (HPI) and Impact on Yttrium-90 (Y-90) Microsphere Therapy, *Journal of Nuclear Medicine, 50* (2009), 2, pp. 214-220
[27] Maus, S., *et al*., Microparticles Based on Biocompatible, Biodegradable Polymers, Possible Surrogates for Y-90 Labelled SIR-Spheres?, *Journal of Nuclear Medicine, 52* (2011), 1, pp. 1594-1600
[28] Patel, U., *et al*., Evaluation of Lung Shunting from Tc-99m MAA Imaging and its Effect to Y-90 Microsphere Treatment Dose, *Journal of Nuclear Medicine, 47* (2006), 1, pp. 555-562
[29] Prasad,V., Baum, R., Long Term Follow-Up of Tubular Renal Function after Peptide Receptor Radionuclide Therapy with Y-90 DOTA-TATE/Lu-177 DOTA-TATE, *Journal of Nuclear Medicine, 49* (2008), 1, pp. 102-108
[30] Prasad, V., *et al*., Survival Benefits and Efficacy of Peptide Receptor Radionuclide Therapy (PRRT) Using Y-90/Lu-177 DOTA-TATE in Pancreatic Neuroendocrine Tumor (pNET), *Journal of Nuclear Medicine, 50* (2009), 2, pp. 43-50
[31] Prasad,V., Baum, R., Renal Toxicity of Two Cycles of Peptide Receptor Radionuclide Therapy (PRRT) as Determined by Serial Measurements of the Glomerular Filtration Rate (GFR) Using Tc-99M DTPA: Comparison between Y-90 DOTA-TATE and Lu-177 DOTA-TATE, *Journal of Nuclear Medicine, 48* (2007), 2, pp. 37-43
[32] Tollefson, C., Krause, S., Nguyen, B., Utility of SPECT/CT Imaging in Y-90 Microsphere Therapy, *Journal of Nuclear Medicine, 56* (2015), 2, pp. 2517-2525

Received on November 18, 2015
Accepted on February 8, 2016

Сеј̂д Мостафа ГАВАМИ, Хосеин ГИАСИ, Асгар МЕСБАХИ

МОНТЕ КАРЛО МОДЕЛОВАЊЕ ПРИМЕНЕ НАНОСФЕРА ИТРИЈУМА-90 ЗА ТЕРАПИЈУ ЈЕТРЕ РАДИОНУКЛИДИМА И ПРОРАЧУН ДОЗА У ОРГАНИМА

Примена радионуклида нанометарских димензија у терапији радионуклидима значајно смањује заустављање честица у ткивима органа и доприноси избегавању настајања тромбозе. Унифромна расподела честица у жељеном органу може бити додатна корист од нанорадионуклида у терапији. Монте Карло симулацијом моделовани математички хумани фантом и ћелије јетре у фантому испуњене су наносферама итријума-90. Процењене су дозе у здравим органима као и фатални и нефатални ризици за околне органе. Процене и прорачуни урађени су за четири различита узорка функције расподеле радионуклида. Максималне дозе и ризици процењени за околне органе утврђени су у моделу јетре са високом концентрацијом у расподели са нанорадионуклидима. Добијене вредности за еквивалентну дозу, ефективну дозу, фаталне и нефаталне ризике износе $7.51\,10^{-3}$ Sv/Bq, $3.01\,10^{-1}$ Sv/Bq, и $9.16\,10^{-1}$ (случајева/10^4 особа), респективно, за бешику, дебело црево и бубрег фантома. Наведене вредности највеће су међу вредностима моделованих расподела. Максималне вредности вероватноће за настанак компликације нормалног ткива здравих органа износе 5.9-8.9 %. У резултатима Монте Карло симулација, примене наночестица итријума-90 показују обећавајућа дозиметријска својства узимајући у обзир извештаје о нетоксичности радионуклида.

Кључне речи: итријум-90, унутрашња дозиметрија, апсорбована доза у органима, процена ризика, терапија радионуклидима